Supplementary Materials: Using Atmospheric Inverse Modelling of Methane Budgets With Copernicus Land Water and Wetness Data to Detect Land Use Related Emissions

Maria K. Tenkanen [1,*], Aki Tsuruta [1], Vilna Tyystjärvi [1], Markus Törmä [2], Iida Autio [2], Markus Haakana [3], Tarja Tuomainen [3], Antti Leppänen [4], Tiina Markkanen [1], Maarit Raivonen [4], Sini Niinistö [5], Ali Nadir Arslan [6] and Tuula Aalto [1]

1. Decomposition of Optimized Methane Emissions to Different Land Cover Classes Using Proportional Corine Land Cover Classes

The CH_4 emission estimates were first assigned to different land cover classes based on the proportional coverage given by the CLC data aggregated to $1° \times 1°$ resolution and keeping the original resolution of CTE-CH_4. When calculating the average CH_4 emission of a land cover class, the CH_4 emissions ([g]) in a single grid cell were first multiplied by the fraction of the land cover class ([%]) in that grid cell, i.e. it was assumed that each land cover class had the same flux per area in a single grid cell and only the proportional fraction differed. These proportional emissions were then summed over the whole of Finland and the sum was divided by the total area of the land cover class ([m^2]) which gave the average annual CH_4 emissions per land cover class area ([g/m^2]).

Confidence intervals for the average CH_4 emissions per land cover class were defined as follows: the CH_4 emissions and the land cover class area per pixel were paired and the pairs were sorted by the magnitude of the CH4 emissions from lowest to highest. The land cover class area was then calculated as a cumulative sum and normalised from zero to one. From the normalised cumulative sum, the values 0.25 and 0.75 were selected and the methane emissions associated with these values were taken as the 25% and 75% confidence intervals. This method selected confidence intervals with the same methane emissions for each land cover class, but weighted them by the area of the land cover class, giving more weight to methane emissions where the land cover class had a larger area.

The process was repeated separately for average annual natural, anthropogenic and total CH_4 emissions to evaluate whether different land cover classes stood out of the rest depending on the CH_4 source as we would expect. From the analysis, we excluded land cover classes that cover less than 0.2% (755 km^2) of the total area of Finland. These classes were 'Forest land, afforested peat', 'Transitional woodland, deforested', 'Transitional woodland, peat, deforested', and 'Wetlands, Marsh'. The exclusion was done to streamline the analysis since it was unexpected that the listed classes would have resulted in reliable results in the machine learning approach given the large difference between the resolution of the inversions and the land cover map.

The range of estimated annual CH_4 fluxes decomposed for selected land cover classes is shown for natural emissions in Figure S5, anthropogenic emissions in Figure S6 and total emissions in Figure S7. The two inversions Inv_{LPX} and Inv_{JSBACH} agreed well with each other, although Inv_{LPX} showed lower natural and consequently lower total CH_4 emissions. The results were similar to those obtained using XGBoost, but there were some notable differences. The main difference is that the magnitude of emissions from different land cover classes was smaller, especially for anthropogenic and total emissions. This is expected as the resolution of $1° \times 1°$ was coarse compared to the resolution and heterogeneity of Corine land cover classes. As can be seen from Figure S8, most land cover classes were correlated with other land cover classes, meaning that there was approximately the same amount of land cover classes in several grid cells. Thus, it was difficult to separate the different categories and the estimated emissions were similar across the land cover classes. However, as was the case with the XGBoost method, the classes "Wetlands, Open bog" and "Transitional woodland, peat" showed elevated CH_4 emissions compared to the other categories.

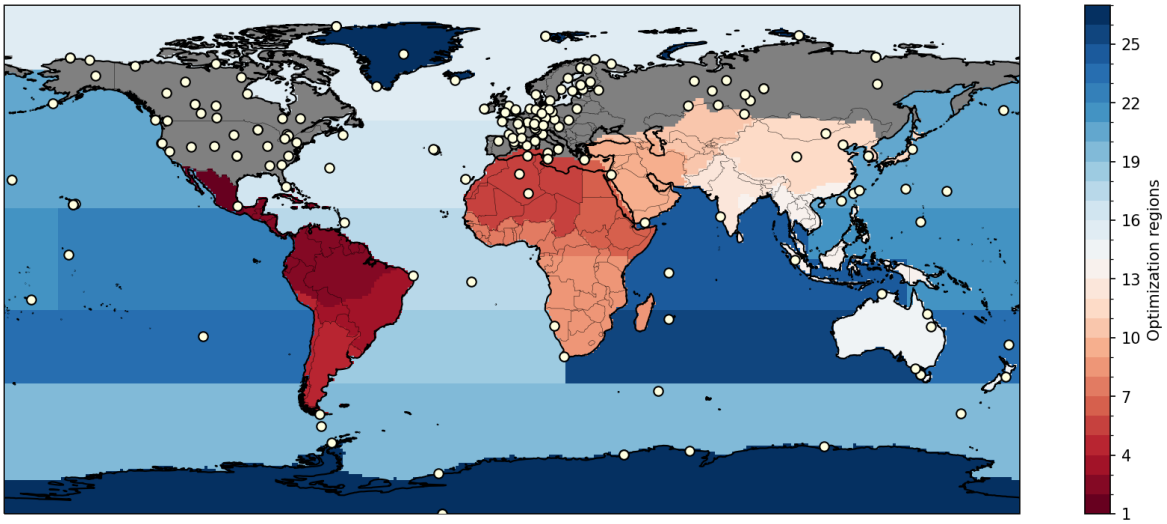

Figure S1. Optimisation regions. The grey region was optimised at 1° latitude × 1° longitude resolution. Circles show the locations of the in situ observation sites from which the concentration observations were used in this study.

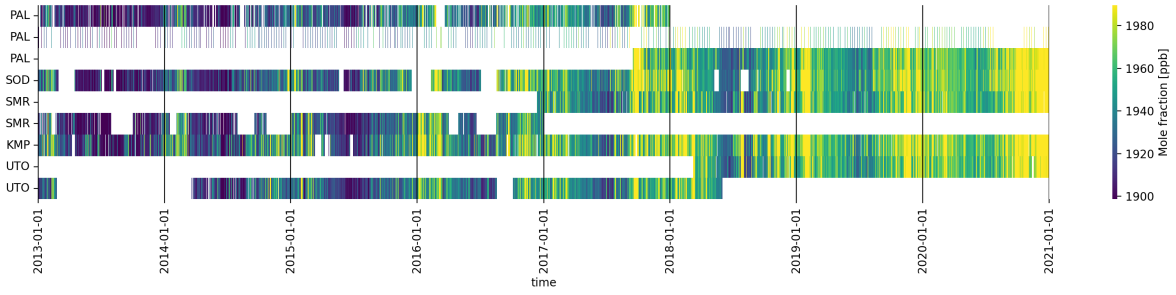

Figure S2. Daily averaged CH_4 mole fraction observations [ppb] in Finnish measurement stations in 2013-2020. The duplicate sites mark the data set before and after the site was included in ICOS. In Pallas, there were also taken flask samples which are shown with discontinuous colour lines.

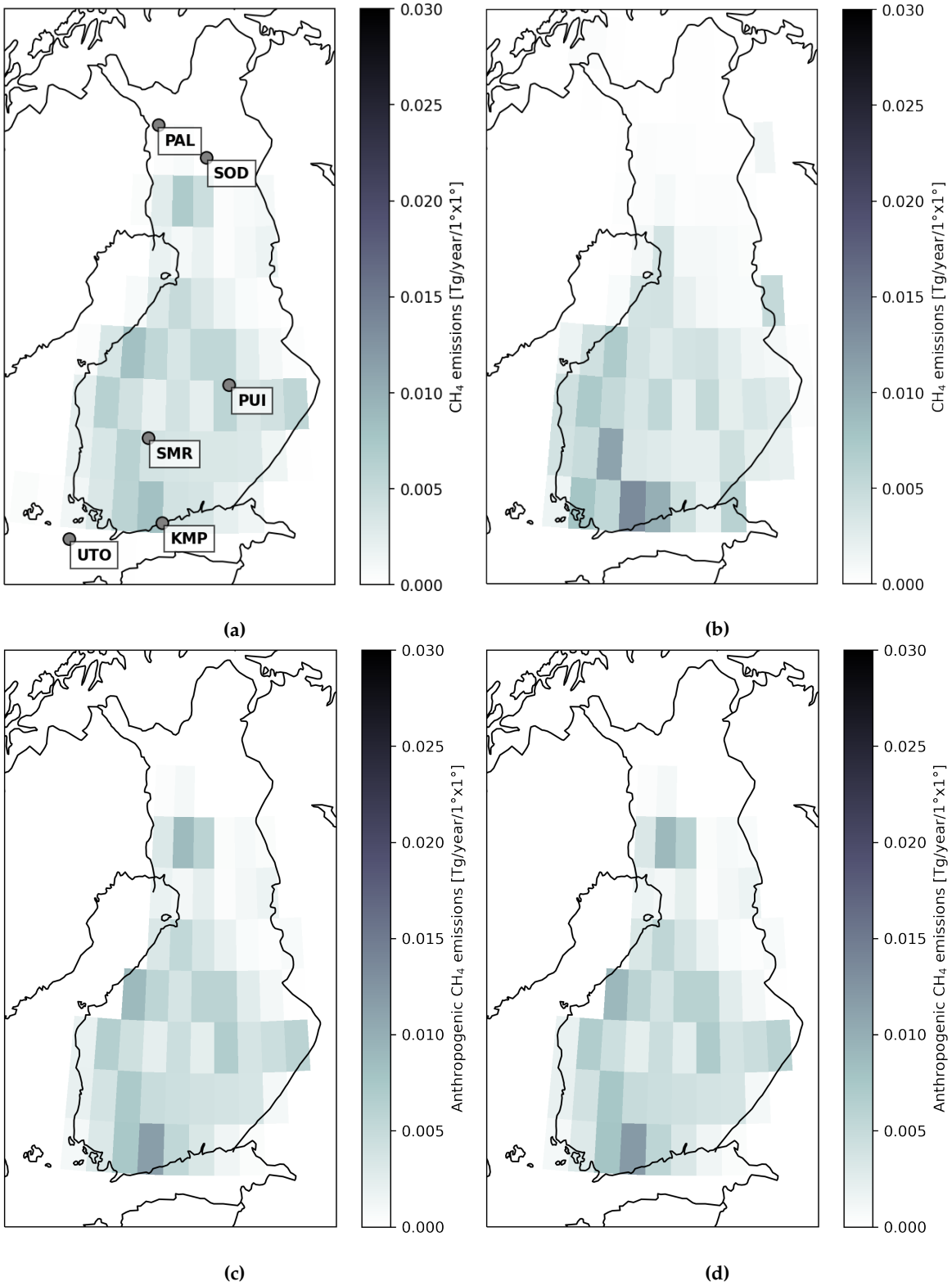

Figure S3. Annual average from 2013–2020 of a) the redistributed CAMS-REG CH_4 emissions, b) the original CAMS-REG, c) the optimised anthropogenic CH_4 emissions from Inv_{JSBACH} and d) the optimised anthropogenic CH_4 emissions from Inv_{LPX}.

Table S1. List of the Finnish surface observation sites used in inversions. Observation Uncertainty (Obs. Unc.) is used to define diagonal values in the observation covariance matrix. The data type is categorized into two measurements (discrete (D) and continuous (C)).

Sitecode	Site Name	Country	Contributor	Longitude [°E]	Latitude [°N]	Height* [m a.s.l.]	Obs. Unc. [ppb]	Data type D/C	Date min.** [year/month]	Date max. [year/month]
KMP	Kumpula	Finland	FMI	24.96	60.20	53.00	30.0	C	2010/01	2019/12
PAL	Pallas-Sammaltunturi, GAW Station	Finland	NOAA	24.12	67.97	570.00	15.0	D	2001/12	2021/03
PAL	Pallas-Sammaltunturi, GAW Station	Finland	FMI	24.12	67.97	570.00	15.0	C	2004/02	2017/12
PAL	Pallas-Sammaltunturi, GAW Station	Finland	ICOS-ATC, FMI	24.12	67.97	577.00	15.0	C	2017/09	2021/04
PUI	Puijo	Finland	FMI	27.66	62.91	84.00	30.0	C	2011/11	2019/12
SMR	Hyytiälä	Finland	ICOS-ATC, UHELS	24.29	61.85	306.00	25.0	C	2016/12	2021/04
SOD	Sodankylä	Finland	FMI	26.64	67.36	227.00	25.0	C	2012/01	2019/12
UTO	Uto	Finland	FMI	21.37	59.78	65.00	25.0	C	2012/03	2018/03
UTO	Uto	Finland	ICOS-ATC, FMI	21.37	59.78	65.00	25.0	C	2018/03	2021/04

*Sampling heights from which atmospheric CH_4 is sampled in TM5. **Observations used in this study between 2010 and 2018.

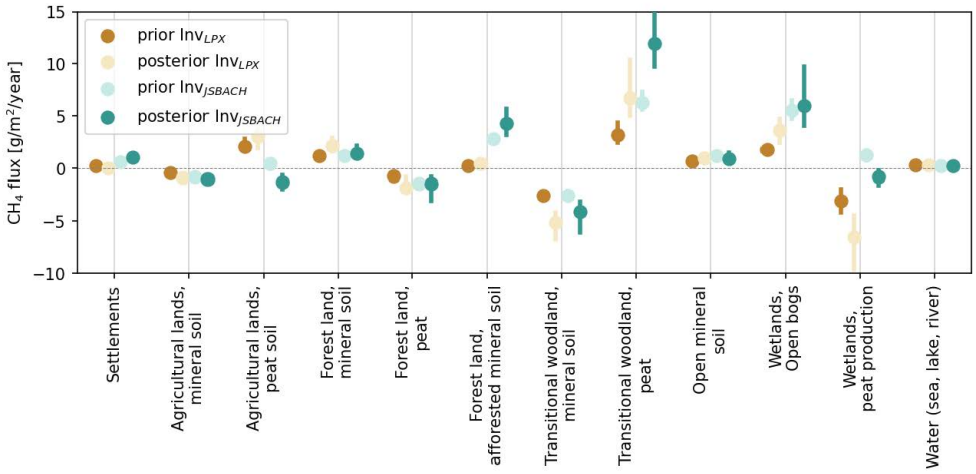

Figure S4. The range of the annual natural CH_4 fluxes (2013–2020) for selected land cover classes estimated with linear regression using prior and optimised natural CH_4 emissions from Inv_{LPX} and Inv_{JSBACH}.

Table S2. List of surface observation sites used in inversions. Observation Uncertainty (Obs. Unc.) is used to define diagonal values in the observation covariance matrix. The data type is categorized into two measurements (discrete (D) and continuous (C)).

Sitecode	Site Name	Country	Contributor	Longitude [°E]	Latitude [°N]	Height* [m a.s.l.]	Obs. Unc. [ppb]	Data type D/C	Date min.** [year/month]	Date max. [year/month]
ABP	Arembepe, Bahia	Brazil	NOAA	-38.17	-12.76	6.00	4.5	D	2006/10	2010/01
ABT	Abbotsford, British Columbia	Canada	EC	-122.34	49.01	93.00	30.0	C	2014/03	2019/06
ALT	Alert, Nunavut	Canada	NOAA	-62.51	82.45	190.00	15.0	D	1999/01	2021/02
ALT	Alert, Nunavut	Canada	EC	-62.51	82.45	195.00	15.0	C	1999/01	2019/07
AMT	Argyle, Maine	United States	NOAA	-68.66	45.01	157.00	30.0	D	2003/09	2006/11
AMY	Anmyeon-do	Republic of Korea	NOAA	126.33	36.54	87.00	30.0	D	2013/12	2021/03
ARA	Arcturus	Australia	CSIRO	148.47	-23.86	185.00	15.0	D	2010/05	2013/10
ASC	Ascension Island	United Kingdom	NOAA	-14.40	-7.97	90.00	15.0	D	1999/01	2021/02
ASK	Assekrem	Algeria	NOAA	5.63	23.26	2715.00	25.0	D	1999/01	2019/11
AZR	Terceira Island, Azores	Portugal	NOAA	-27.36	38.76	24.00	15.0	D	1999/01	2021/02
AZV	Azovo	Russian Federation	NIES	73.03	54.71	190.00	30.0	C	2009/10	2018/12
BAL	Baltic Sea	Poland	NOAA	16.67	55.35	28.00	75.0	D	1999/01	2011/06
BAR	Baranova	Russian Federation	FMI	101.62	79.28	30	4.5	C	2015/11	2020/12
BCK	Behchoko, Northwest Territories	Canada	EC	-115.92	62.80	220.00	15.0	C	2010/10	2019/06
BHD	Baring Head Station	New Zealand	NOAA	174.87	-41.41	90.00	4.5	D	2002/03	2020/08
BIK	Bialystok	Poland	MPIBGC	23.01	53.23	483.00	25.0	C	2005/07	2014/06
BIR	Birkenes	Norway	NILU	8.25	58.39	219	25.0	C	2009/05	2018/12
BKT	Bukit Kototabang	Indonesia	NOAA	100.31	-0.20	875.00	75.0	D	2004/01	2021/03
BLK	Baker Lake, Nunavut	Canada	EC	-96.01	64.33	61.00	15.0	C	2017/07	2019/07
BME	St. Davids Head, Bermuda	United Kingdom	NOAA	-64.65	32.37	17.00	15.0	D	1999/01	2010/01
BMW	Tudor Hill, Bermuda	United Kingdom	NOAA	-64.88	32.26	33.00	15.0	D	1999/01	2021/03
BRA	Bratt's Lake Saskatchewan	Canada	EC	-104.71	50.20	630.00	75.0	C	2009/10	2019/07
BRW	Barrow Atmospheric Baseline Observatory	United States	NOAA	-156.61	71.32	27.46	15.0	C	1999/01	2021/04
BRW	Barrow Atmospheric Baseline Observatory	United States	NOAA	-156.58	71.32	16.00	15.0	D	1999/01	2021/03
BRZ	Berezorechka	Russian Federation	NIES	84.33	56.15	248.00	75.0	C	2008/05	2018/12
BSC	Black Sea, Constanta	Romania	NOAA	28.66	44.18	5.00	75.0	D	1999/01	2011/12
BSD	Bilsdale	United Kingdom	UNIVBRIS	-1.15	54.36	628.00	30.0	C	2014/01	2019/12
CBA	Cold Bay, Alaska	United States	NOAA	-162.71	55.21	25.00	15.0	D	1999/01	2021/04
CBY	Cambridge Bay, Nunavut Territory	Canada	EC	-105.06	69.13	47.00	15.0	C	2012/12	2019/07
CDL	Candle Lake, Saskatchewan	Canada	EC	-105.12	53.99	630.00	30.0	C	2002/06	2008/01
CFA	Cape Ferguson	Australia	CSIRO	147.06	-19.28	5.00	25.0	D	1991/06	2021/04
CGO	Cape Grim, Tasmania	Australia	NOAA	144.68	-40.68	164.00	4.5	D	1999/01	2021/02
CGO	Cape Grim	Australia	CSIRO	144.68	-40.68	94.00	15.0	C	2012/07	2021/07
CGR	Charles Point, Darwin	Australia	CSIRO	12.65	37.67	9.00	25.0	C	2015/04	2018/12
CHL	Churchill, Manitoba	Canada	EC	-93.82	58.74	89.00	15.0	C	2011/10	2019/07
CHM	Chibougamau, Quebec	Canada	EC	-74.34	49.69	423.00	30.0	C	2007/08	2011/04
CHR	Christmas Island	Republic of Kiribati	NOAA	-157.15	1.70	5.00	15.0	D	1999/01	2020/01
CIB	Centro de Investigacion de la Baja Atmosfera	Spain	NOAA	-4.93	41.81	850.00	25.0	D	2009/05	2021/03
CMN	Mt. Cimone Station	Italy	UNIURB	10.68	44.17	2172.00	15.0	C	2008/07	2017/12
CMN	Mt. Cimone Station	Italy	ICOS-ATC,CNR-ISAC	10.70	44.19	2173.00	15.0	C	2018/05	2021/05
CPS	Chapais,Quebec	Canada	EC	-74.98	49.82	431.00	15.0	C	2011/12	2019/07
CPT	Cape Point	South Africa	NOAA	18.49	-34.35	260.00	25.0	D	2010/02	2021/03
CRI	Cape Rama	India	CSIRO	73.83	15.08	66.00	75.0	D	1993/02	2013/01
CRV	Carbon in Arctic Reservoirs Vulnerability Expe...	United States	NOAA	-147.60	64.99	643.13	15.0	C	2011/10	2021/05
CRZ	Crozet Island	France	NOAA	51.85	-46.43	202.00	4.5	D	1999/01	2020/11
CUR	Monte Curcio	Italy	IIA	16.42	39.32	1801.00	15.0	C	2014/12	2017/12
CYA	Casey Station, Antarctica	Australia	CSIRO	110.52	-66.28	55.00	4.5	D	1997/06	2021/01
DEM	Demyanskoe	Russian Federation	NIES	70.87	59.79	155.00	30.0	C	2005/09	2018/12
DRP	Drake Passage	Drake Passage	NOAA	-61.68	-59.07	10.00	4.5	D	2006/03	2020/12
DSI	Dongsha Island	Taiwan	NOAA	116.73	20.70	8.00	15.0	D	2010/03	2021/03
DVV	Danville, Virginia	United States	PSU	-79.44	36.71	492.00	15.0	C	2016/07	2017/12
EGB	Egbert, Ontario	Canada	EC	-79.78	44.23	276.00	25.0	C	2005/03	2019/06
EIC	Easter Island	Chile	NOAA	-109.45	-27.13	72.00	4.5	D	1999/01	2019/11
ENA	Eastern North Atlantic, Graciosa, Azores	Portugal	LBNL-ARM	-28.03	39.09	40.48	25.0	C	2015/07	2019/12
ESP	Estevan Point, British Columbia	Canada	EC	-126.54	49.38	47.00	25.0	C	2009/03	2019/07
EST	Esther, Alberta	Canada	EC	-110.21	51.67	757.00	30.0	C	2010/01	2019/07
ETL	East Trout Lake, Saskatchewan	Canada	EC	-104.99	54.35	598.00	30.0	C	2005/08	2019/07
FNE	Fort Nelson, British Columbia	Canada	EC	-122.57	58.84	376.00	30.0	C	2014/07	2019/07
FSD	Fraserdale	Canada	EC	-81.57	49.88	250.00	30.0	C	1999/01	2019/07
GAT	Gartow	Germany	ICOS-ATC,HPB	11.44	53.07	411.00	25.0	C	2016/05	2021/05
GCI	Millerville, AL	United States	PSU	-85.89	33.18	428.00	25.0	C	2017/10	2018/05
GMI	Mariana Islands	Guam	NOAA	144.66	13.39	8.00	15.0	D	1999/01	2021/03
GPA	Gunn Point	Australia	CSIRO	131.04	-12.25	37.00	75.0	D	2010/08	2021/02
HBA	Halley Station, Antarctica	United Kingdom	NOAA	-26.21	-75.61	35.00	4.5	D	1999/01	2020/02
HEI	Heidelberg	Germany	IUP	8.68	49.42	143.00	30.0	C	2005/01	2014/09
HNP	Hanlan's Point, Ontario	Canada	EC	-79.39	43.61	97.00	25.0	C	2014/06	2019/04
HPB	Hohenpeissenberg	Germany	NOAA	11.02	47.80	941.00	25.0	D	2006/04	2021/03
HPB	Hohenpeissenberg	Germany	ICOS-ATC,HPB	11.02	47.80	1065.00	25.0	C	2015/09	2021/05
HSU	Humboldt State University	United States	NOAA	-124.44	41.57	7.60	30.0	D	2008/05	2017/05
HTM	Hyltemossa	Sweden	ICOS-ATC,LUND-CEC	13.42	56.10	265.00	25.0	C	2017/04	2021/04
HUN	Hegyhatsal	Hungary	NOAA	16.65	46.95	344.00	25.0	D	1999/01	2021/01
HUN	Hegyhatsal	Hungary	HMS	16.65	46.95	344.00	75.0	C	2006/03	2014/10
ICE	Storhofdi, Vestmannaeyjar	Iceland	NOAA	-20.29	63.40	121.70	15.0	D	1999/01	2021/02
IGR	Igrim	Russian Federation	NIES	64.41	63.19	89.00	30.0	C	2005/04	2013/07
INU	Inuvik,Northwest Territories	Canada	EC	-133.53	68.32	123.00	15.0	C	2012/02	2019/07
IPR	Ispra	Italy	ICOS-ATC,JRC	8.64	45.81	310.00	30.0	C	2017/12	2021/04
IZO	Izana, Tenerife, Canary Islands	Spain	NOAA	-16.48	28.30	2377.90	25.0	D	1999/01	2021/02
JFJ	Jungfraujoch	Switzerland	EMPA	7.99	46.55	3580.00	15.0	C	2014/01	2017/12
JFJ	Jungfraujoch	Switzerland	ICOS-ATC,HFSJG	7.99	46.55	3585.00	15.0	C	2016/12	2021/04
KEY	Key Biscayne, Florida	United States	NOAA	-80.20	25.67	6.00	25.0	D	1999/01	2021/02

*Sampling heights from which atmospheric CH_4 is sampled in TM5. **Observations used in this study between 2010 and 2018.

Table S2. Continuation to the table S2.

Sitecode	Site Name	Country	Contributor	Longitude [°E]	Latitude [°N]	Height* [m a.s.l.]	Obs. Unc. [ppb]	Data type D/C	Date min.** [year/month]	Date max. [year/month]
KIT	Karlsruhe	Germany	ICOS-ATC,HPB	8.42	49.09	310.00	30.0	C	2016/12	2021/04
KJN	Kjolnes	Norway	Univ. Exeter	29.23	70.85	20	15.0	C	2013/10	2018/08
KRE	Kresin u Pacova	Czech Republic	ICOS	15.08	49.57	784.00	25.0	C	2017/04	2021/04
KRS	Karasevoe	Russian Federation	NIES	82.42	58.25	156.00	30.0	C	2004/09	2018/12
KUM	Cape Kumukahi, Hawaii	United States	NOAA	-155.01	19.51	3.00	15.0	D	1999/01	2021/04
KZD	Sary Taukum	Kazakhstan	NOAA	75.57	44.45	600.00	75.0	D	1999/01	2009/08
KZM	Plateau Assy	Kazakhstan	NOAA	77.87	43.25	2524.00	25.0	D	1999/01	2009/08
LEF	Park Falls, Wisconsin	United States	NOAA	-90.27	45.95	868.00	30.0	C	2010/09	2021/05
LEF	Park Falls, Wisconsin	United States	NOAA	-90.26	45.95	868.00	30.0	D	1999/01	2021/04
LIN	Lindenberg	Germany	ICOS-ATC,HPB	14.12	52.17	171.00	30.0	C	2015/10	2021/05
LLB	Lac La Biche, Alberta	Canada	NOAA	-112.45	54.95	546.10	30.0	D	2008/01	2013/02
LLB	Lac La Biche, Alberta	Canada	EC	-112.47	54.95	590.00	30.0	C	2007/04	2019/07
LLN	Lulin	Taiwan	NOAA	120.86	23.47	2867.00	25.0	D	2006/08	2021/04
LMP	Lampedusa	Italy	NOAA	12.63	35.52	50.00	25.0	D	2006/10	2021/02
LMP	Lampedusa	Italy	ICOS-ATC,ENEA	12.63	35.52	53.00	25.0	C	2020/01	2021/04
LMT	Lamezia Terme	Italy	ISAC	16.23	38.88	14.00	30.0	C	2015/01	2016/12
LPO	Ile Grande	France	LSCE	-3.58	48.80	20.00	15.0	D	2005/01	2013/08
LUT	Lutjewad	Netherlands	ICOS-ATC,RUG	6.35	53.40	61.00	25.0	C	2018/08	2021/04
MAA	Mawson, Antarctica	Australia	CSIRO	62.87	-67.62	32.00	4.5	D	1984/04	2021/02
MEX	High Altitude Global Climate Observation Center	Mexico	NOAA	-97.31	18.98	4469.00	15.0	D	2009/01	2021/02
MHD	Mace Head, County Galway	Ireland	NOAA	-9.90	53.32	26.00	25.0	D	1999/01	2021/03
MID	Sand Island, Midway	United States	NOAA	-177.38	28.21	8.00	15.0	D	1999/01	2021/03
MKN	Mt. Kenya	Kenya	NOAA	37.30	-0.06	3649.00	25.0	D	2003/12	2011/06
MLO	Mauna Loa, Hawaii	United States	NOAA	-155.58	19.54	3437.00	15.0	C	1999/01	2021/04
MLO	Mauna Loa, Hawaii	United States	NOAA	-155.58	19.54	3402.00	15.0	D	1999/01	2021/04
MNM	Minamitorishima	Japan	JMA	153.98	24.29	27.10	15.0	C	1999/01	2019/12
MQA	Macquarie Island	Australia	CSIRO	158.97	-54.48	13.00	4.5	D	1990/04	2021/02
MRC	Marcellus Pennsylvania	United States	PSU	-76.42	41.47	652.00	75.0	C	2015/05	2019/01
NAT	Farol De Mae Luiza Lighthouse	Brazil	NOAA	-35.19	-5.51	20.00	15.0	D	2010/09	2020/03
NGL	Neuglobsow	Germany	UBA	13.03	53.14	62.00	75.0	C	2005/01	2013/12
NMB	Gobabeb	Namibia	NOAA	15.01	-23.58	461.00	25.0	D	1999/01	2021/02
NOR	Norunda	Sweden	ICOS-ATC,LUND-CEC	17.48	60.09	146.00	15.0	C	2017/04	2021/04
NOY	Noyabrsk	Russian Federation	NIES	75.78	63.43	188.00	30.0	C	2005/10	2018/12
NWR	Niwot Ridge, Colorado	United States	NOAA	-105.57	40.05	3526.00	15.0	D	1999/01	2021/04
OPE	Observatoire perenne de l'environnement	France	ICOS-ATC,LSCE	5.50	48.56	510.00	30.0	C	2016/08	2021/04
OTA	Otway Basin	Australia	CSIRO	142.82	-38.52	50.00	30.0	D	2005/09	2014/08
OXK	Ochsenkopf	Germany	NOAA	11.81	50.03	1185.00	30.0	D	2003/03	2019/06
OXK	Ochsenkopf	Germany	ICOS-ATC,HPB	11.81	50.03	1185.00	30.0	C	2019/09	2021/04
PDM	Pic du Midi	France	LSCE	0.14	42.94	2887.00	15.0	D	2005/02	2018/02
POC	Pacific Ocean	Pacific Ocean	NOAA	-130.75	0.12	20.00	15.0	D	1999/01	2017/07
PSA	Palmer Station, Antarctica	United States	NOAA	-64.05	-64.77	15.00	4.5	D	1999/01	2020/12
PTA	Point Arena, California	United States	NOAA	-123.74	38.95	22.00	25.0	D	1999/01	2011/05
PUY	Puy de Dome	France	ICOS-ATC,LSCE	2.97	45.77	1475.00	15.0	C	2016/08	2021/05
RGL	Ridge Hill	United Kingdom	UNIVBRIS	-2.54	52.00	294.00	25.0	C	2012/02	2019/12
RPB	Ragged Point	Barbados	NOAA	-59.43	13.16	20.00	15.0	D	1999/01	2021/03
RUN	La Réunion	France	ICOS-ATC,LSCE	55.38	-21.08	2160.00	15.0	C	2018/05	2021/04
RYO	Ryori	Japan	JMA	141.82	39.03	280.00	15.0	C	1999/01	2019/12
SAC	Saclay	France	ICOS-ATC,CEA	2.14	48.72	260.00	75.0	C	2017/05	2021/04
SCT	Beech Island, South Carolina	United States	NOAA	-81.83	33.41	420.20	75.0	C	2015/08	2021/05
SDZ	Shangdianzi	China	NOAA	117.12	40.65	298.00	15.0	D	2009/09	2015/09
SEY	Mahe Island	Seychelles	NOAA	55.53	-4.68	7.00	15.0	D	1999/01	2020/12
SGP	Southern Great Plains, Oklahoma	United States	NOAA	-97.50	36.62	339.00	75.0	D	2002/04	2021/04
SGP	Southern Great Plains, Oklahoma	United States	LBNL-ARM	-97.49	36.61	374.00	75.0	C	2010/11	2020/01
SHM	Shemya Island, Alaska	United States	NOAA	174.08	52.72	28.00	25.0	D	1999/01	2021/03
SMO	Tutuila	American Samoa	NOAA	-170.56	-14.23	60.30	15.0	D	1999/01	2021/03
SNB	Sonnblick	Austria	EAA	47.05	12.96	3111.00	15.0	C	2012/04	2018/12
SPO	South Pole, Antarctica	United States	NOAA	-24.80	-89.96	2821.30	4.5	D	1999/01	2021/01
SSL	Schauinsland	Germany	UBA-Germany	7.92	47.90	1217.00	30.0	C	2004/12	2018/12
STE	Steinkimmen	Germany	ICOS-ATC,HPB	8.46	53.04	281.00	75.0	C	2019/07	2021/04
STM	Ocean Station M	Norway	NOAA	2.00	66.00	5.00	25.0	D	1999/01	2009/11
SUM	Summit	Greenland	NOAA	-38.42	72.60	3214.54	15.0	D	2000/08	2020/08
SVB [1]	Svartberget	Sweden	ICOS-ATC,SLU	19.77	64.26	419.00	25.0	C	2017/06	2021/04
SYO	Syowa Station, Antarctica	Japan	NOAA	39.59	-69.00	16.00	4.5	D	1999/01	2021/01
TAC	Tacolneston	United Kingdom	NOAA	1.14	52.52	236.00	25.0	D	2014/06	2016/01
TAP	Tae-ahn Peninsula	Republic of Korea	NOAA	126.13	36.73	21.00	75.0	D	1999/01	2021/02
THD	Trinidad Head, California	United States	NOAA	-124.15	41.05	112.00	25.0	D	2002/04	2017/06
TIK	Hydrometeorological Observatory of Tiksi	Russia	NOAA	128.89	71.60	29.00	15.0	D	2011/08	2018/09
TIK	Tiksi	Russian Federation	FMI	128.89	71.60	29.00	15.0	C	2010/09	2019/12
TOH	Torfhaus	Germany	ICOS-ATC,HPB	10.53	51.81	948.00	25.0	C	2017/12	2021/04
TPD	Turkey Point, Ontario	Canada	EC	-80.56	42.64	266.00	25.0	C	2012/11	2019/07
TRN	Trainou	France	ICOS-ATC,LSCE	2.11	47.96	311.00	25.0	C	2016/08	2021/04
USH	Ushuaia	Argentina	NOAA	-68.31	-54.85	32.00	4.5	D	1999/01	2021/03
UTA	Wendover, Utah	United States	NOAA	-113.72	39.90	1332.00	25.0	D	1999/01	2021/04
UUM	Ulaan Uul	Mongolia	NOAA	111.10	44.45	1012.00	25.0	D	1999/01	2020/10
VGN	Vaganovo	Russian Federation	NIES	62.32	54.50	277.00	30.0	C	2008/06	2018/12
VKV	Voeikovo	Russian Federation	MGO	30.70	59.95	76.00	25.0	C	2008/05	2014/12
WIS	Weizmann Institute of Science at the Arava Ins...	Israel	NOAA	35.06	29.96	482.00	25.0	D	1999/01	2021/04
WKT	Moody, Texas	United States	NOAA	-97.32	31.31	256.00	75.0	D	2001/03	2006/11
WLG	Mt. Waliguan	Peoples Republic of China	NOAA	100.90	36.27	3890.00	15.0	D	1999/01	2020/12
WPC	Western Pacific Cruise	Western Pacific	NOAA	143.70	0.13	10.00	15.0	D	2004/12	2013/06
WSA	Sable Island, Nova Scotia	Canada	EC	-60.01	43.93	8.00	25.0	C	2003/06	2019/07
YAK	Yakutsk	Russian Federation	NIES	129.36	62.09	344.00	30.0	C	2007/09	2013/12
YON	Yonagunijima	Japan	JMA	123.01	24.47	50.00	30.0	C	1999/02	2019/12
ZEP	Ny-Alesund, Svalbard	Norway and Sweden	NOAA	11.89	78.91	479.00	15.0	D	1999/01	2021/03
ZEP	Ny-Alesund, Svalbard	Norway and Sweden	ICOS-ATC,NILU	11.89	78.91	489.00	15.0	C	2017/07	2021/04
ZOT	Zottino	Russian Federation	MPIBGC	89.21	60.48	415.00	25.0	C	2009/05	2016/12
ZOT	Zottino	Russian Federation	MPIBGC	89.21	60.48	415.00	15.0	D	2006/10	2013/06
ZSF	Zugspitze / Schneefernerhaus	Germany	UBA-Germany	10.98	47.42	2670.00	30.0	C	2004/12	2019/12

*Sampling heights from which atmospheric CH_4 is sampled in TM5. **Observations used in this study between 2010 and 2018.

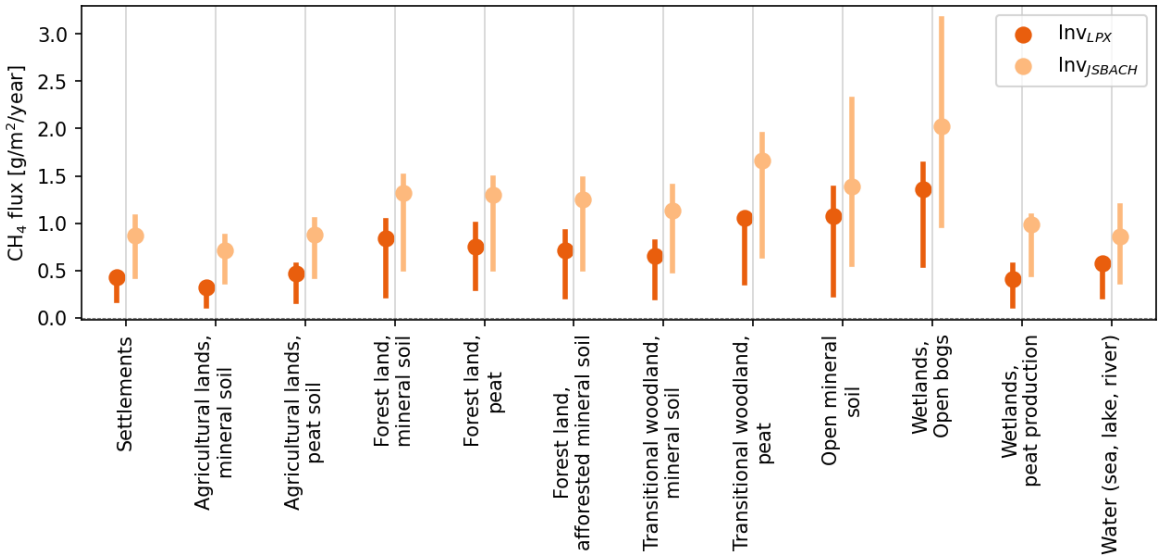

Figure S5. The range of annual natural CH_4 fluxes (2013–2020) decomposed for selected land cover classes estimated using proportional Corine land cover classes.

2. Using Machine Learning to Estimate LULUCF Methane Emissions

To detect LULUCF-related CH_4 emissions from the inversion model estimate, we used a machine learning model called gradient boosting. Gradient boosting trains multiple decision trees on a random subset of data, and the predictions of all trees are combined to produce a final result. This ensemble method is more accurate than a single decision tree and is less prone to overfitting. Gradient boosting is also robust to outliers and can perform automatic feature selection. We used a gradient boost library called XGBoost [2].

We trained the machine learning model with annual natural, anthropogenic and total CH_4 emissions estimates from Inv_{JSBACH} and Inv_{LPX}. The training was conducted in a resolution of 10 km $\times$ 10 km. The training and predicting of the CH_4 emissions were done separately for each year 2013–2020.

The fraction of each land cover class was calculated at 10 km $\times$ 10 km and all the land cover classes were used as features in the training of the machine learning model. The annual CH_4 emissions were resampled to the same resolution using kd-tree nearest neighbour approach in Python package called pyresample [3] and then used as the target value. With the trained model, we estimated the annual emissions for a grid cell that was occupied by only one land cover class. From the analysis, we excluded land cover classes that cover less than 0.2% (755 km^2) of the total area of Finland. These classes were 'Forest land, afforested peat', 'Transitional woodland, deforested', 'Transitional woodland, peat, deforested', and 'Wetlands, Marsh'.

When the machine learning algorithm XGBoost was trained with optimised annual natural CH_4 emission estimates in Finland and the CH_4 emissions were estimated by a land cover class, the two

inversions, Inv_{JSBACH} and Inv_{LPX}, mostly agreed (Figure S9). The two land cover classes with the highest predicted natural emissions were 'Transitional woodland, peat' and 'Wetland, Open bogs'. Another notable feature was 'Forest, mineral soil', which showed higher emissions than the other classes with Inv_{LPX}. 'Forest land' in general was also higher when Inv_{JSBACH} was used. This was probably an artefact from the machine learning approach and the coarse resolution of CTE-CH_4. 'Forest land, mineral soil' is the most prominent land cover class by a large margin covering almost a third of the area in Finland. It also correlated with almost all the other land cover classes (Figure S8), meaning forests existed near almost all land cover types. This led to a situation where there were always forests in grid cells with high CH_4 emissions. Additionally, Inv_{JSBACH} showed a larger land sink on mineral soils than Inv_{LPX}. These differences alongside the highlighted land cover types were reasonable given the land cover data the priors used. In addition, in some years XGBoost predicted a CH_4 sink for some land cover types on mineral soil. This was more pronounced with Inv_{JSBACH} than with Inv_{LPX}.

The average natural CH_4 emission on 'Transitional woodland, peat' predicted by the XGBoost was 1.7 g/m^2/year with LPX and 2.0 g/m^2/year with JSBACH. Even though these values are higher than the emissions factor for the poorly drained forests, they are still reasonable, especially when the range of observed values is considered [4].

When the machine learning model was trained with annual anthropogenic CH_4 emissions, 'Settlements' was the most prominent class (Figure S10). Predicted emissions in other classes were close to zero, with agricultural lands showing a bit larger emissions.

The XGBoost predicted CH_4 emissions trained with annual total emissions resembled the combination of the natural and anthropogenic emission results (Figure S11): the natural and anthropogenic sources listed above ('Transitional woodland, peat', 'Wetland, Open bogs', 'Settlements' and 'Forest land, mineral soil') were elevated from the rest of the land cover classes.

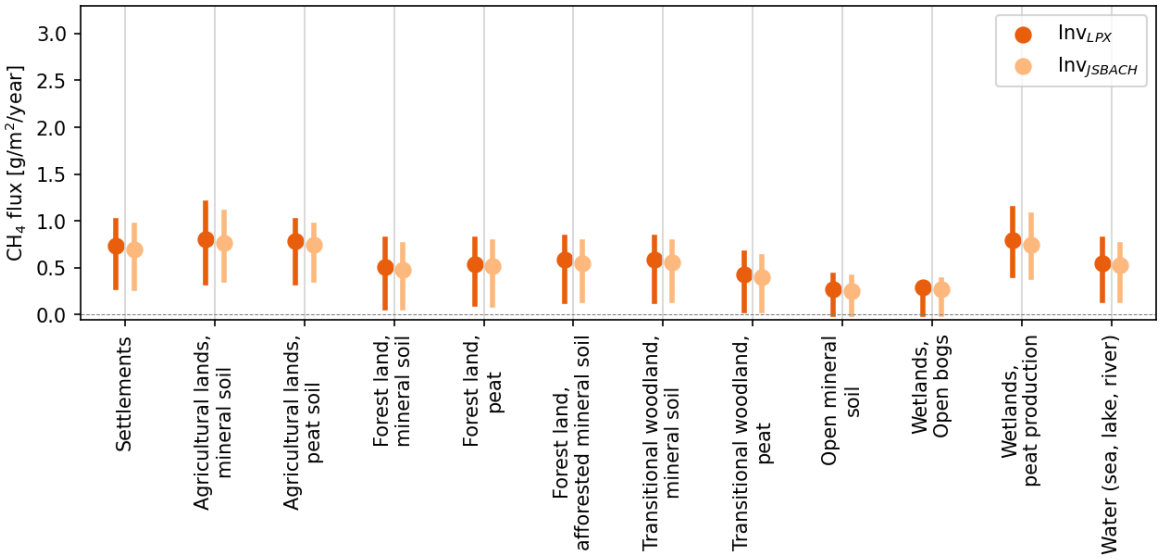

Figure S6. The range of annual anthropogenic CH_4 fluxes (2013–2020) decomposed for selected land cover classes estimated using proportional Corine land cover classes.

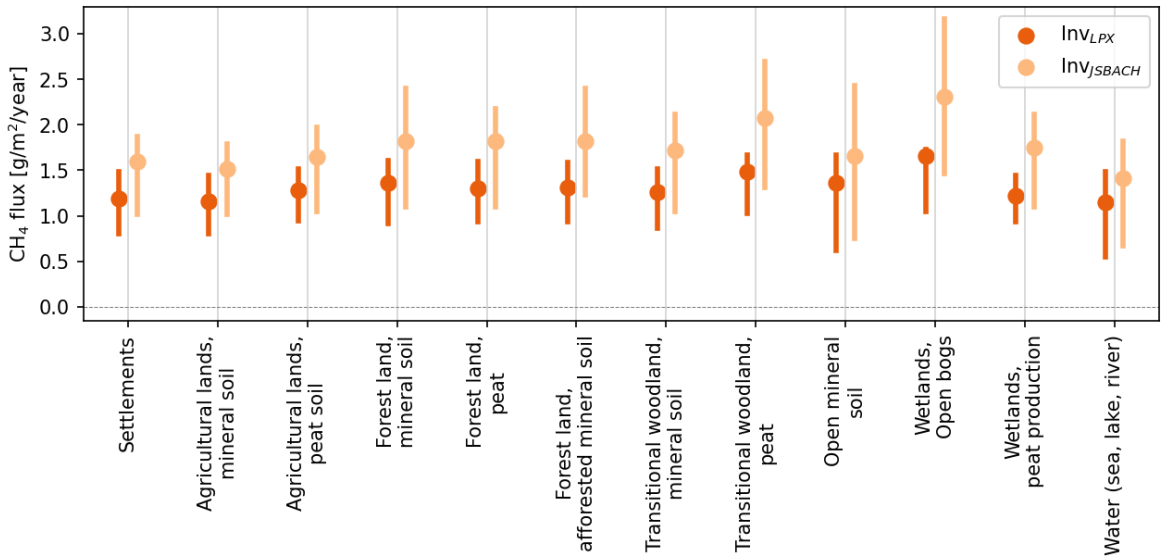

Figure S7. The range of annual total CH_4 fluxes (2013–2020) decomposed for selected land cover classes estimated using proportional Corine land cover classes.

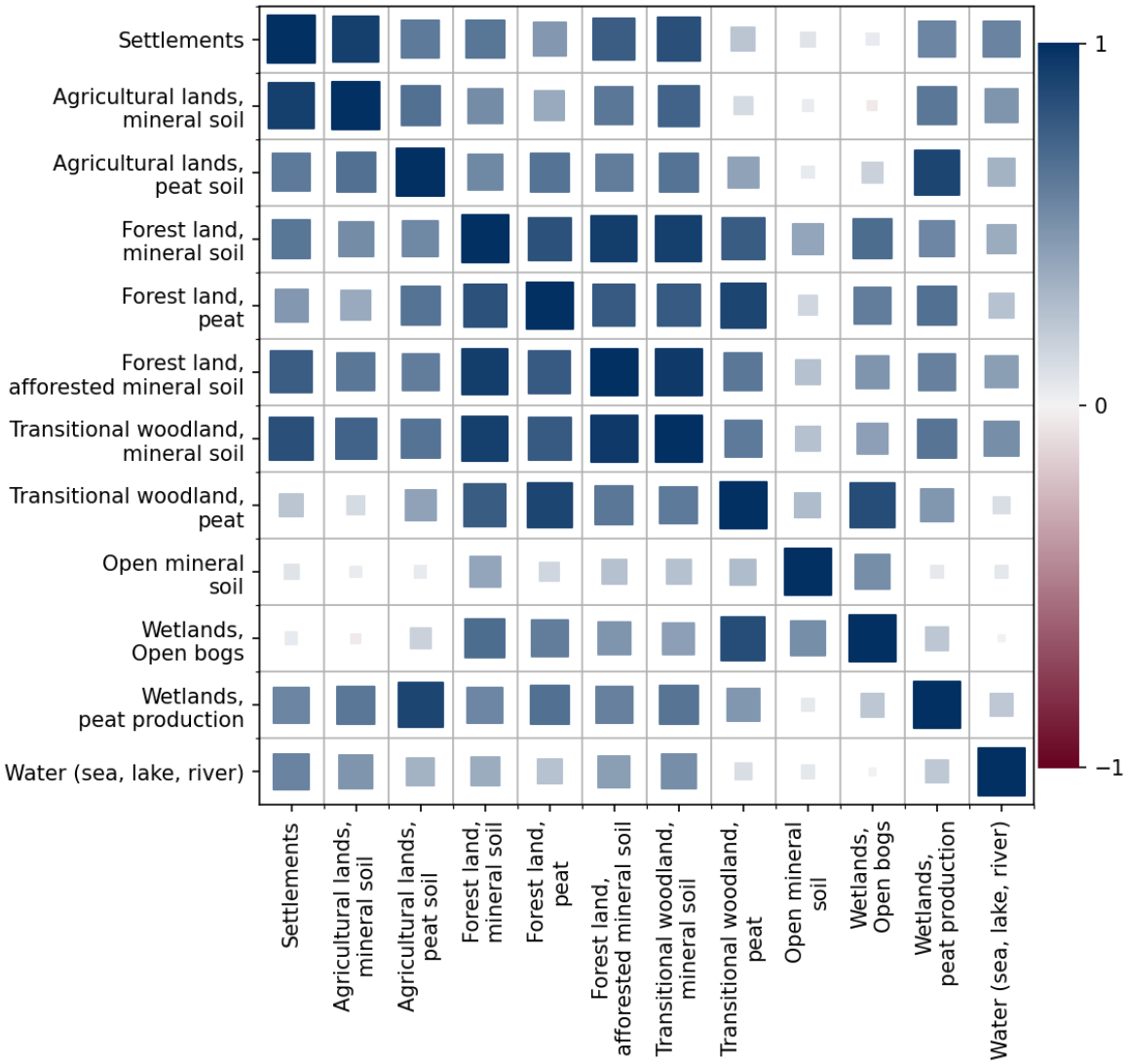

Figure S8. Pairwise Pearson correlation coefficient of the selected Corine land cover classes at a resolution of 1° × 1° in Finland. The colour of a square is related to the correlation coefficient and the size to the absolute value of the coefficient: an absolute value would fill the cell and a zero value would mean that there would be no square.

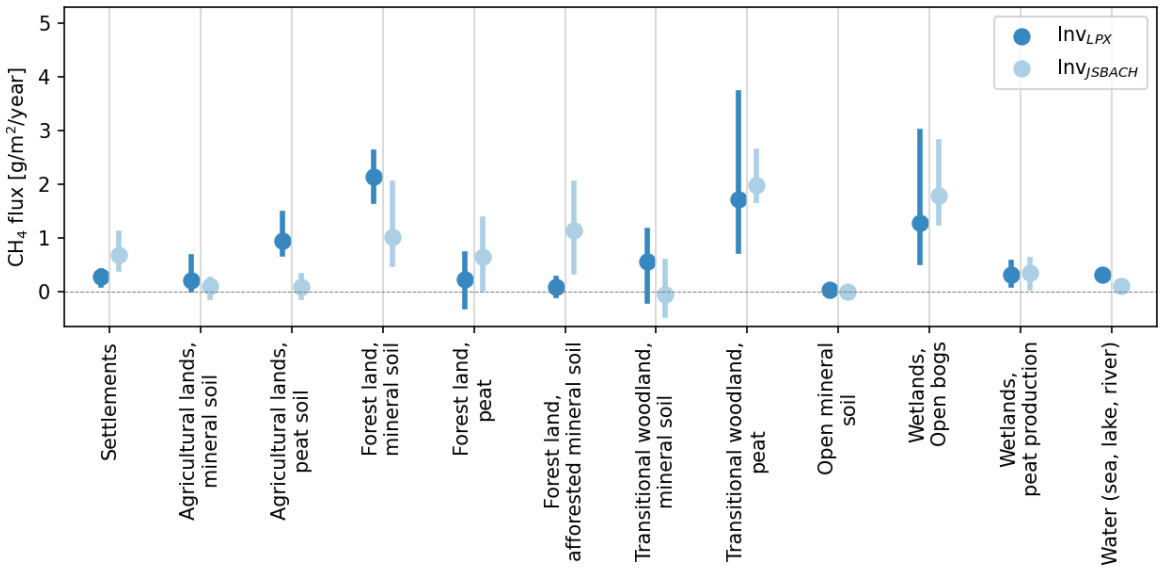

Figure S9. The range of the annual natural CH_4 fluxes (2013–2020) for selected land cover classes estimated with XGBoost using optimised natural CH_4 emissions from Inv_{LPX} and Inv_{JSBACH}.

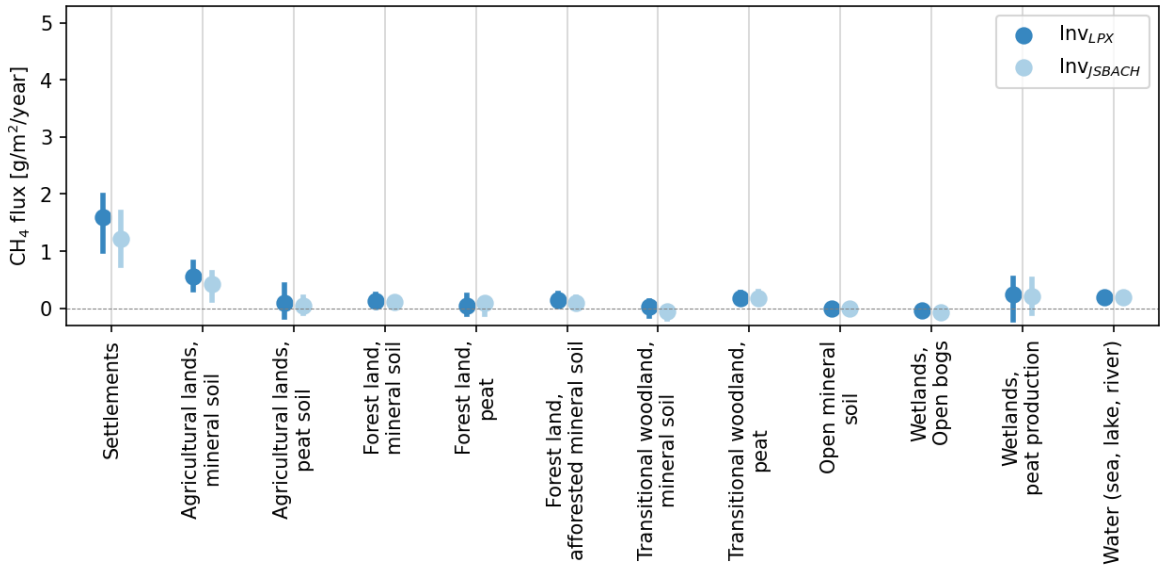

Figure S10. The range of annual anthropogenic CH_4 fluxes (2013–2020) for selected land cover classes estimated with XGBoost using optimised anthropogenic CH_4 emissions from Inv_{LPX} and Inv_{JSBACH}.

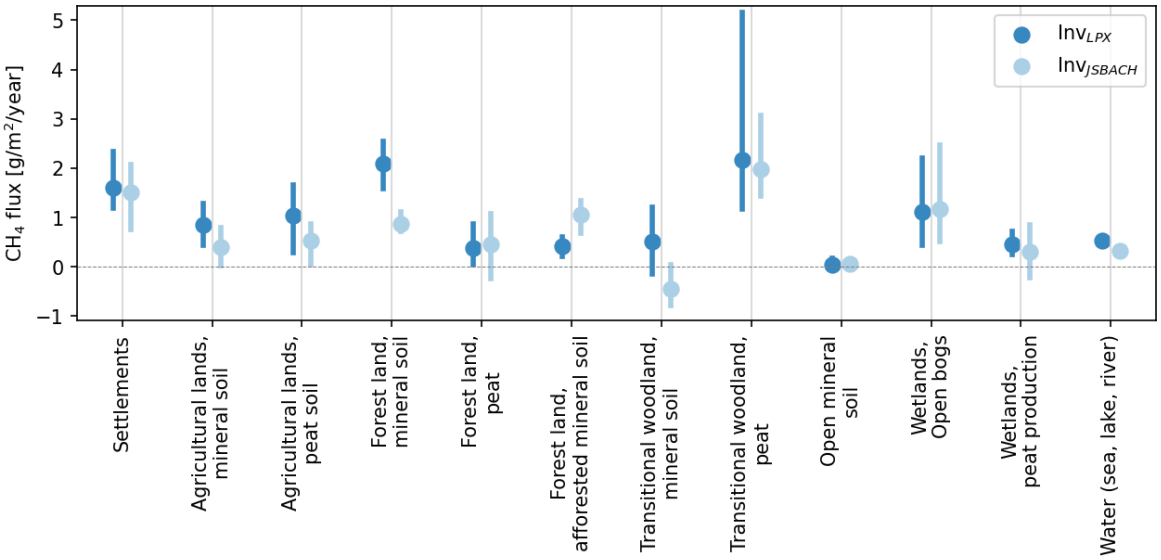

Figure S11. The range of annual total CH_4 fluxes (2013–2020) for selected land cover classes estimated with XGBoost using optimised total CH_4 emissions from Inv_{LPX} and Inv_{JSBACH}.

References

1. Marklund, P.; Ottosson-Löfvenius, M.; Smith, P. ICOS ATC CH4 Release, Svartberget (150.0 m), 2017-06-01–2022-02-28, 2022.
2. Chen, T.; Guestrin, C. XGBoost: A Scalable Tree Boosting System. Proceedings of the 22nd ACM SIGKDD International Conference on Knowledge Discovery and Data Mining; ACM: New York, NY, USA, 2016; Vol. 42, pp. 785–794. doi:10.1145/2939672.2939785.
3. Hoese, D.; Raspaud, M.; Lahtinen, P.; Roberts, W.; Lavergne. pytroll/pyresample: Version 1.16.0., 2020. doi:10.5281/zenodo.3372769.
4. Ojanen, P.; Minkkinen, K.; Alm, J.; Penttilä, T. Soil–atmosphere CO2, CH4 and N2O fluxes in boreal forestry-drained peatlands. *Forest Ecology and Management* **2010**, *260*, 411–421. doi:10.1016/j.foreco.2010.04.036.